applied sciences

MDPI

Article

Influence of Improved Particle Breakage Index on Deformation Strength Characteristics of Soil-Rock Mixtures

Ping Xu *, Zeliang Chen, Lingyun Fang, Zengguang Xu, Qingwei Lin and Zhilong Liu

State Key Laboratory of Eco-Hydraulics in Northwest Arid Region, Xi'an University of Technology, Xi'an 710048, China; chenzeliang2024@163.com (Z.C.); fly1836478971@163.com (L.F.); xuzengguang@xaut.edu.cn (Z.X.); linqingwei19999@163.com (Q.L.); 17868518198@163.com (Z.L.)
* Correspondence: xuping1986@xaut.edu.cn

Abstract: A large-scale triaxial shear test was performed on a waste slag dam created from the accumulation of waste slag during the construction of a pumped-storage power station. By integrating previous experience, the particle breakage index was refined to study the relationship between particle breakage and the deformation strength characteristics of the soil-rock mixture under different dry densities and stress states. The results show that as the confining pressure increases, various dry densities enhance particle breakage, leading to a transition from initial dilatancy to shear shrinkage in the soil-rock mixture. This change results in a decrease in the nonlinear internal friction angle and a decrease in the shear strength. This research explores the shear failure mechanism caused by the breakage of soil-rock mixtures. Examination of the particle grade before and after shearing shows that the extent of particle breakage expands with higher confining pressure, especially within the 20~60 mm grain size range. The fractal dimension is calculated concurrently, showing a strong correlation with the breakage index. The concepts of the phase transition stress ratio and failure dilatancy ratio were applied to describe the deformation characteristics. Experimental results demonstrate that the influence of the phase transition stress ratio on the dilatancy becomes more significant with increased dry density, yet this effect diminishes with higher confining pressure. As the breakage index increases, the failure dilatancy rate decreases following a power function, resulting in a gradual reduction in the dilatancy phenomenon. Considering the substantial influence of clay particles on the cohesion of the soil-rock mixture and the negligible effect of breakage on fine particles, it is proposed that the cohesion remains unchanged for determining the friction parameter. With increasing breakage index, the internal friction angle decreases nonlinearly, weakening the shear strength. This analysis shows that the refined particle breakage index effectively captures the particle breakage characteristics of soil-rock mixtures, providing valuable insights into the deformation and strength characteristics of engineering structures affected by particle breakage.

Keywords: improved particle breakage index; nonlinear internal friction angle; soil-rock mixture; large-scale triaxial shear test

check for updates

Citation: Xu, P.; Chen, Z.; Fang, L.; Xu, Z.; Lin, Q.; Liu, Z. Influence of Improved Particle Breakage Index on Deformation Strength Characteristics of Soil-Rock Mixtures. *Appl. Sci.* **2024**, *14*, 5899. https://doi.org/10.3390/app14135899

Academic Editor: Tiago Miranda

Received: 15 May 2024
Revised: 30 June 2024
Accepted: 3 July 2024
Published: 5 July 2024

Copyright: © 2024 by the authors. Licensee MDPI, Basel, Switzerland. This article is an open access article distributed under the terms and conditions of the Creative Commons Attribution (CC BY) license (https://creativecommons.org/licenses/by/4.0/).

1. Introduction

In the construction of pumped-storage power stations, a significant quantity of waste slag is generated, forming a loose structure that is prone to particle breakage under load. This can lead to changes in the slag's gradation and structure, ultimately affecting overall stability. Hazardous conditions such as strong rains and floods can trigger landslides, mud/rock flows, and other geological disasters, posing serious threats to both property and safety. Therefore, an experimental study is currently underway to analyze the characteristics of particle breakage and the development of soil-rock mixtures under load. The aim is to gain insights that can be used to address the safety and stability concerns associated with waste slag dams.

An accurate characterization of the extent of particle breakage is essential for analyzing the patterns of particle breakage. The particle breakage index serves as an effective tool for

assessing the degree of particle breakage. Marsal [1] proposed the breakage index B_g as a measure of overall particle breakage. B_g is a fundamental, easily accessible, and widely applicable metric. However, it does not accurately represent the specific changes occurring within each particle group. Hardin [2] introduced the concept of the relative breakage rate B_r, which takes into account the overall variations in the particle size distribution during breakage. Hardin's relative breakage rate B_r offers a more direct quantification of particle breakage compared to the breakage index B_g. Nevertheless, it should be noted that not all particles undergo breakage, which deviates from real-world conditions. Einav [3] introduced the notion of a limit grading curve, defining the particle breakage potential S_g as the area between the limit grading curve and the initial grading curve [4]. The limit grading index B_E, ranging from 0 to 1, is suitable for comparing and evaluating the degree of particle breakage in different soils. However, determining the ultimate grading curve of the soil sample requires additional testing, which can be challenging. Guo et al. [5] examined the equation for the ultimate grading breakage index B_E and proposed a new breakage index, B_W. This new index, which captures the characteristics of the original grading curve, reduces the need for extensive experimental calculations of the ultimate grading curve, offering a simpler and more practical solution. The value range of the breakage index, from 0 to infinity, is not suitable for comparing the degree of particle breakage. By summarizing the advantages and disadvantages of the above breakage indexes, the latest breakage index, B_W, can be modified to better express the degree of particle breakage and used for particle breakage comparison.

Scholars [6–9] have recently conducted comprehensive tests to describe the mechanical characteristics and parameters that influence soil-rock mixtures. In one study, Tu et al. [7] performed extensive direct shear testing on soil-rock mixtures with varying stone percentages. They were able to establish a correlation between the relative breakage rate, normal stress, and stone content. The results indicate that particle breakage increases with increasing normal stress and stone content. Another study by Lei et al. [8] utilized laboratory testing to develop a direct shear numerical model for analyzing the strength parameters of soil-rock mixtures. They also quantified particle breakage and demonstrated a hyperbolic connection with normal stress. Microscopic analysis revealed that the soil-rock mixture experiences both tensile and shear failure under shear stress.

Despite compositional differences, previous academic studies [10–15] on soil-rock mixtures and similar materials have shown consistent mechanical characteristics. These findings offer valuable insights for further research on soil-rock mixtures. SUITS et al. [10] and Jiang et al. [11] studied the effect of scaling on the shear strength of coarse-grained soil and reported that the shear strength index is strongly influenced by the particle size. Cai et al. [12] investigated the particle breakage of rockfill during triaxial shear testing under varying conditions of gradation, relative density, and confining pressure. Their findings demonstrated that particle breakage is significantly affected by gradation and confining pressure. They developed a relationship function based on fractal dimension to analyze the strength and dilatancy characteristics of the gradation and confining pressure. Additionally, Guo et al. [13] developed a relationship between the breakage index and the gradation equation using the concept of the gradation equation. They established an evolution model of gradation with stress–strain by establishing a relationship function between the breakage index and stress–strain state. This model can be used to predict the change in the particle breakage process during the shear stage. Liang et al. [15] established the repeated compaction characteristic curve of graded macadam through repeated compaction and screening of graded macadam. The correlation between fractal dimension of particle size distribution and repeated compaction times, water content, and dry density were analyzed.

Particle breakage in granular soil-rock mixtures is a critical engineering parameter that significantly influences their strength and deformation characteristics [16–18]. A precise characterization of this parameter is essential for analyzing the engineering strength and stability of such mixtures. To gain a better understanding of the particle breakage law during

triaxial shearing of soil-rock mixtures, the breakage index B_W, introduced by Guo et al. [5], is enhanced to more accurately measure the particle breakage characteristics. This improvement aims to simplify the particle breakage index test and facilitate a comparative evaluation of the degree of particle breakage. Furthermore, a fractal dimension will be employed to validate the test's validity. The dilatancy characteristics will be elucidated by examining the phase transition stress ratio under different dry density and confining pressure conditions. The gradations before and after shear will also be analyzed. This paper investigates the deformation strength characteristics of soil-rock mixtures using an improved breakage index, B_C. The concept of the failure dilatancy rate is introduced, demonstrating the correlation between the breakage index and failure dilatancy rate and explaining its dilatancy behavior. This study establishes a link between the breakage index and the nonlinear internal friction angle to demonstrate the shear strength of the sample.

2. Introduced the Improved Particle Breakage Index B_C

2.1. Improved the Definition of the Breakage Index

The particle breakage index is a quantitative measure used to characterize the degree and properties of particle breakage. With regard to the breakage index B_W suggested by Guo et al. [5]:

$$B_W = \frac{S_1 - S_0}{S_0} \tag{1}$$

The modified curve captures the characteristics of the original grading curve and minimizes the need for additional experimental calculations of the limit grading curve, making it a simple and practical solution. However, because the breakage index B_W ranges from 0 to infinity, it is not suitable for comparing or evaluating the degree of particle breakage. To address this limitation, the following improvements are made to the B_W suggested by Guo et al. [5]. Based on this, the breakage index B_C is proposed:

$$B_C = \frac{S_1 - S_0}{S_1} \tag{2}$$

where the starting grading curve is S_0, the grading curve after the test is S_1, and the area enclosed by the maximum particle size is $d = d_{max}$. As shown in Figure 1.

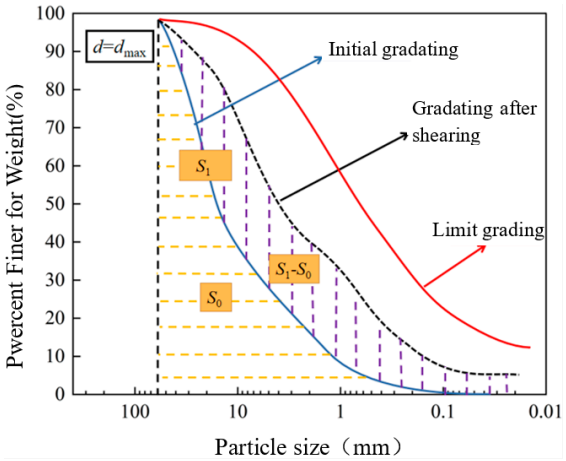

Figure 1. Schematic diagram of the definition of the current breakage, B_W and B_C.

The theoretical value range of B_C is defined as between 0 and 1. A value of $B_C = 0$ indicates an unbroken state, while $B_C = 1$ signifies full breakage and reflects the complete shift in gradation. This revised index is straightforward and practical. Muir Wood et al. [19] introduced the breakage index I_G, which is calculated as the ratio of the area between the shear particle-grading curve and the maximum particle size line to the area between the limit particle-grading curve and the maximum particle size line. Although the forms of B_C and I_G may differ, their underlying cores are identical.

2.2. Improve the Quantitative Correlation between the Breakage Index B_C and Fractal Dimension D

The concept of fractals was introduced by Mandelbrot [20] to explain the complex geometric patterns observed in nature. In the context of a mixture of earth and rock, internal particles experience uneven breakage when subjected to external loads. As a result, fractal dimension, a measure of complexity within fractal geometry, is used to objectively characterize particle breakage and determine the relationship between breakage and strength [21]. Tyler et al. [22] assumed that particle groups of varying sizes shared the same density and developed a mathematical model for particle fractal dimension.

$$lg\left[\frac{M(\rho < d_i)}{M_T}\right] = (3 - D)lg\left(\frac{d_i}{d_{max}}\right) \tag{3}$$

where $M(\rho < d_i)$ represents the particle mass below a specific scale; M_T is the total mass of particles in the sample; and d_{max} is the largest particle size in the sample.

$lg\left(\frac{d_i}{d_{max}}\right)$ is plotted on the x-axis, and $lg\left[\frac{M(\rho<d_i)}{M_T}\right]$ is plotted on the y-axis, based on linear regression fitting a straight line with slope k in a type $3 - D$ graph. The slope k is determined to calculate the score dimension D [23].

The particle size d_i ranges from a minimum value of 0 mm to a maximum value that represents 100% soil content. When calculating the area using integration, the integral of P is taken over the interval $[i, 1]$. Then, let k approach 0 and find the limit, as shown in Figure 2. The grading curve area is represented in P-lg$d$ coordinates:

$$S = \lim_{i \to 0} S_A = \int_i^1 (lgd_{max} - lgd_i)dP \tag{4}$$

where d_i is the particle size that corresponds to $P = i$.

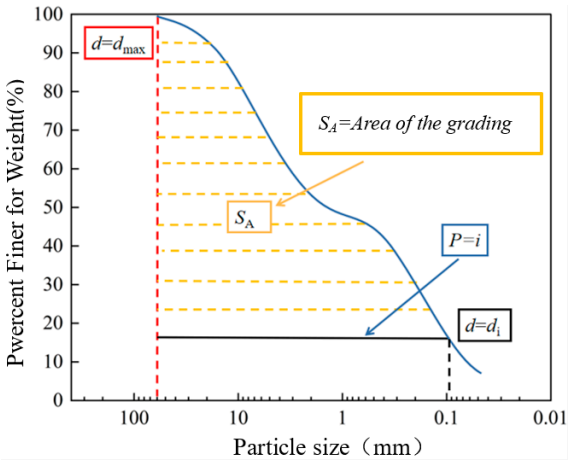

Figure 2. Schematic diagram of calculation area of gradation equation.

By manipulating Equation (3) for the fractal dimension, we can derive:

$$lgd_{max} - lgd_i = -\frac{1}{3-D}lgP \tag{5}$$

Replacing Equation (5) with Equation (4):

$$S = \lim_{i \to 0} S_A = \int_i^1 \left(-\frac{1}{3-D}lgP\right)dP \tag{6}$$

$$S = \lim_{i \to 0} S_A = \left(-\frac{1}{3-D}\right)\int_i^1 \left(\frac{\ln P}{\ln 10}\right)dP \tag{7}$$

$$S = \lim_{i \to 0} S_A = \left(-\frac{1}{3-D}\right)\left(\frac{1}{\ln 10}\right)\int_i^1 (\ln P)dP \tag{8}$$

By performing integration by parts as i approaches 0, we observe:

$$\lim_{i \to 0} P = \int_i^1 (\ln P) dP = -1 \tag{9}$$

Replacing Equation (9) with Equation (8) results in:

$$S = \frac{1}{(\ln 10)(3-D)} \tag{10}$$

Replacing Equation (10) with Equation (2) results in:

$$B_C = \frac{\frac{1}{\ln 10}\left(\frac{1}{3-D_c} - \frac{1}{3-D_0}\right)}{\frac{1}{\ln 10}\left(\frac{1}{3-D_c}\right)} \tag{11}$$

Condense to:

$$B_C = \frac{D_c - D_0}{3-D_0} \tag{12}$$

where D_C represents the fractal dimension of the current gradation, D_0 represents the fractal dimension of the beginning gradation, and D_C and D_0 can be determined using the fractal dimension of the test.

Equation (12) [24] establishes the relationship between the breakage index B_C and the fractal dimension D_C of the current gradation, serving as a transformation link.

3. Large-Scale Triaxial Test on the Shear Failure Characteristics of a Soil-Rock Mixture

3.1. Experimental Procedures

The soil-rock mixture material is extracted from the waste slag dam filling material generated during the construction of a pumped-storage power station in Northwest China, as depicted in Figure 3. The garbage disposal area utilizes this material. The slag dump site is a perennial ditch with a discharge of 0.5 m^3/s. The width of the ditch bottom is generally 8~13 m. The lithology on both sides is granodiorite and the width of the valley bottom is generally more than 20 m. The lithology on both sides is Sinian Dengying Formation striated marble. Due to the limitation of topographic conditions, the construction slag forms several small-scale spoil yards, the maximum height difference is less than 100 m, and the actual confining pressure is less than 1 MPa. In order to study the accuracy of its mechanical properties, the sample is analyzed with large size and small confining pressure in this triaxial test. Figure 4 shows the test materials. The sample has a stone composition of 52%, a measured natural water content of 10%, and an average specific gravity (G_S) of 2.83. Representative samples were obtained using the quartering method, and the grading curve was plotted. The obtained sample exhibits discontinuous gradation. Due to the limitation of the test size, the original gradation is adjusted using the equivalent replacement approach.



Figure 3. Construction site drawing of the slag dump.



Figure 4. Test material.

The equivalent replacement approach involves substituting large particles with soil particles that are smaller than the maximum allowable particle size of the instrument but larger than 5 mm in proportion and with equal mass. The objective is to closely preserve the mechanical characteristics of the scaled material to the original grading constituents by controlling the amount of fine material present. The equipment can accommodate particles up to 60 mm in size. The scaled grading curve is shown in Figure 5.

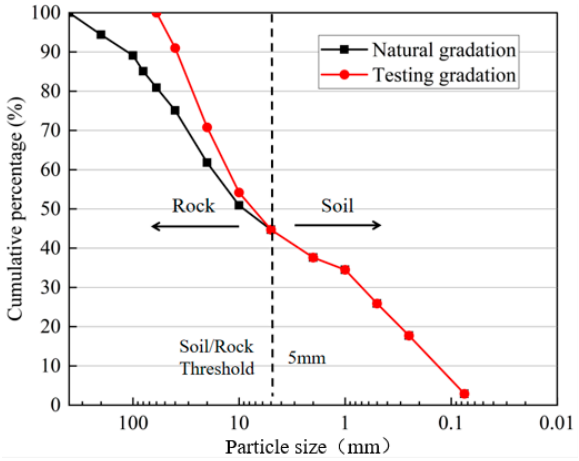

Figure 5. Grading curve of the S-RM before shearing.

The minimum dry density of the sample was determined using the fixed-volume method to fill the sample cylinder. The sample height was measured using a shaking table, and the sample volume was calculated to obtain the maximum dry density. The design code points out that "the filling standard of gravel and sand should take the relative density as the design control index". Referring to the actual design standard of the project, this paper chooses the relative density of 0.6 as the sample preparation control. Different sample dry densities are generated based on the maximum dry density and the minimum dry density. The initial void ratio e_0 of the sample was determined through conversion. The test and calculation results are displayed in Table 1.

Table 1. Relative density test results.

Test Number	Minimum Dry Density g/cm^3	Maximum Dry Density g/cm^3	Sample Dry Density g/cm^3	Initial Void Ratio e_0
1	1.65	1.85	1.76	0.61
2	1.71	1.91	1.82	0.55
3	1.82	2.15	2.00	0.42
4	1.98	2.28	2.15	0.32
5	2.16	2.39	2.30	0.23

The triaxial test employs a large triaxial compression tester with a sample size of ϕ300 × H600 mm, a maximum confining pressure of 3.0 MPa, a maximum axial stress of 21 MPa, a maximum stroke of 300 mm, and a shear rate of 0.4 mm/min, as illustrated in Figure 6.



Figure 6. Triaxial testing machine.

Five groups of unsaturated isotropic consolidated drainage (CD) shear tests with different dry densities (ρ_d = 1.76, 1.82, 2.00, 2.15, and 2.30 g/cm^3) were conducted, and the confining pressures were 100, 200, 400, and 800 kPa, respectively. Sample preparation was carried out according to the grain gradation after scaling down the soil-rock mixture as described in Figure 5, and the sample mass is calculated according to the dry density and the size of the sample cylinder. The prepared sample is mixed until the coarse and fine particles are uniform, packed into a molding cylinder covered with rubber film in layers, and vibrated for compaction to prevent the separation of coarse and fine particles, and the interface between layers is chiseled to reduce the influence of the interlayer effect on shearing. After the sample loading is completed, the test device applied a constant vertical stress, and the drainage system was used to remove water from the soil sample to achieve isotropic consolidation. Shear stress was then applied when the required degree of consolidation was reached. After the test, the sample was air-dried and screened, and a postshear grading curve was drawn. The laboratory tests yielded stress-axial strain curves, volumetric strain-axial strain curves, and shear strength parameters of the soil-rock mixture. These tests were conducted to explore the changing law of particle breakage through grading changes before and after shearing.

3.2. Analysis of the Stress-Strain Relationship Curve

Figure 7 displays the stress-axial strain curves and volumetric strain-axial strain curves of the soil-rock mixture at various confining pressures during a triaxial test. According to the Standard for Geotechnical Test Methods (GB/T 50123-2019) [25], the stress corresponding to the axial strain of 15–20% is usually taken as the failure stress in the hardening curve. The axial strain corresponding to the failure stress is 15% in this test. As the dry density remains constant, the failure stress increases with increasing confining pressure. Moreover, as the dry density increases, the failure stress tends to increase as well. During the initial phase of the test, the specimen undergoes shrinkage followed by dilatancy, resulting in an increase in the volume as the dry density increases. As the confining pressure increases, the specimen's dilatancy exhibits hysteresis, transitioning from shear dilatation to shear shrinkage, ultimately leading to a decrease in the volume variable. Manzari et al. [26] suggested that this behavior can be explained by the state-dependent dilatancy characteristics of bulk particles, specifically the phase transition stress ratio $M_{pt} = q/p$ (where q represents the critical dilatancy stress and p is the average primary stress). Figure 8

displays the phase transition stress for various dry densities at varying confining pressures. It is evident from Figure 8 that the phase transition stress ratio increases with increasing dry density under a specific confining pressure, resulting in an increase in the volume. Conversely, as the confining pressure increases, the phase transition stress ratio gradually decreases at a constant dry density, indicating a steady decrease in the volume variable. This finding corroborates the previously stated conclusion.

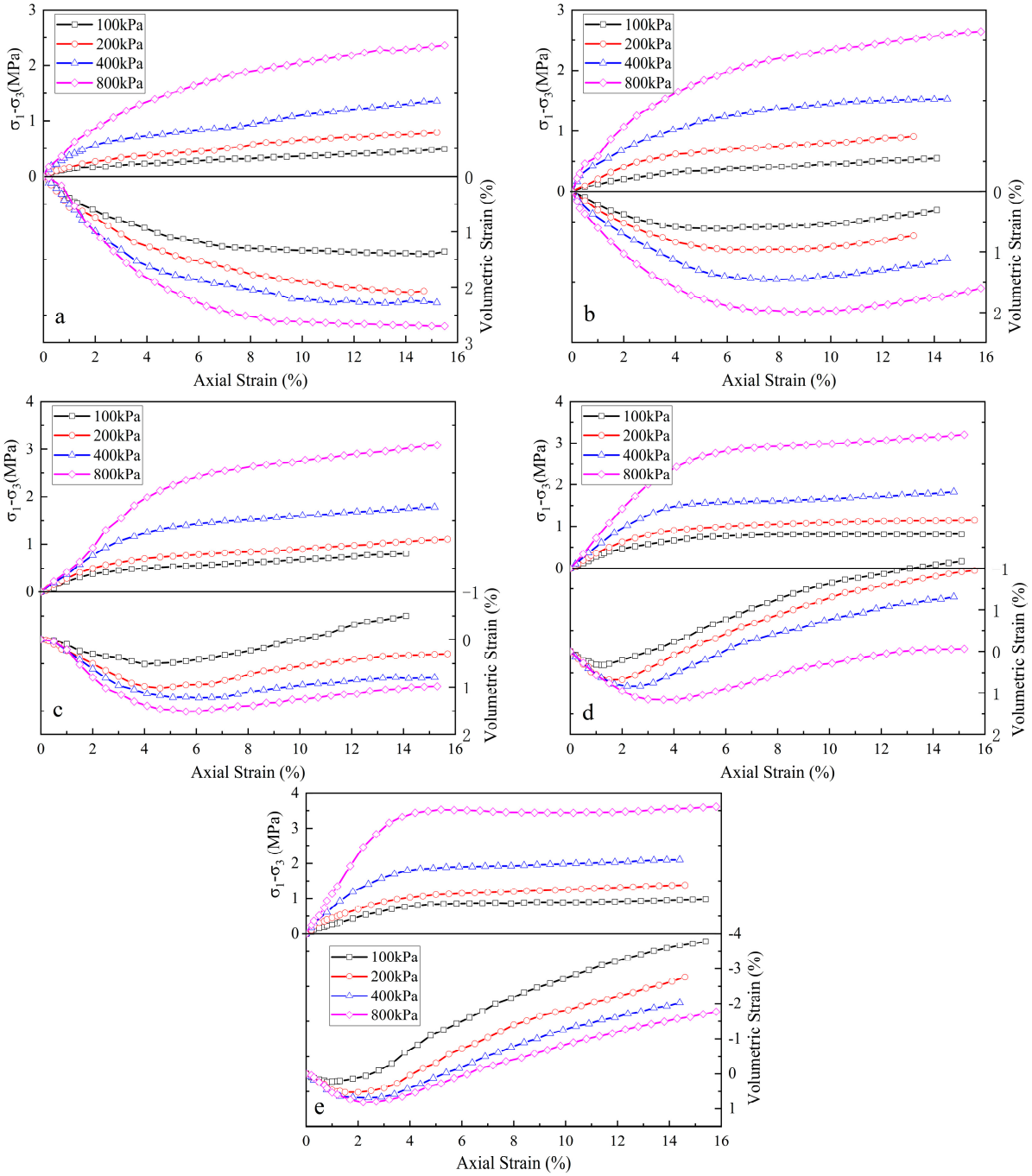

Figure 7. Stress–strain relations of different types of samples in the triaxial tests: (**a**) dry density of 1.76 g/cm^3, (**b**) dry density of 1.82 g/cm^3, (**c**) dry density of 2.00 g/cm^3, (**d**) dry density of 2.15 g/cm^3, and (**e**) dry density of 2.30 g/cm^3.

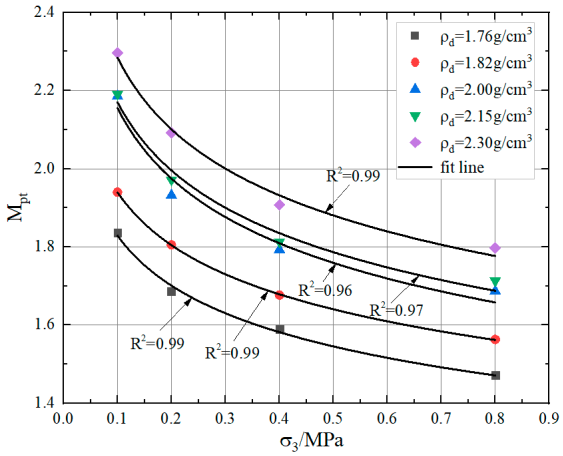

Figure 8. Relationship between M_{pt} and σ_3.

3.3. Analyzing the Particle-Grading Curves before and after Shearing at Various Dry Densities

The waste slag dam filling material primarily consists of marble and granodiorite, which are known for their high strength and complex composition. To examine the failure mechanism, the sheared sample was air-dried and sifted. Figure 9 presents the grading curves before and after shearing at different dry densities, while Table 2 provides the grading findings of the soil-rock mixture after shearing. The results clearly indicate particle breakage during the triaxial shear process. With increasing confining pressure, the grading curve shifts upward, indicating an increase in particle breakage [27,28]. The "dilatation" among the particle groups on the grading curve becomes more pronounced as the dry density increases. Notably, the sample with a dry density of 2.30 g/cm^3 exhibited a more significant change in the particle size distribution than did the sample with a dry density of 1.76 g/cm^3. This suggests that particle breakage becomes more pronounced as the dry density increases. That is, with increasing dry density, the sample becomes denser, the contact between particles increases, the occlusal arrangement increases, and it rolls and breaks under the action of shear [29].

For analysis, a single dry density of 2.00 g/cm^3 is taken into consideration. Figure 10 shows the content histogram of each particle group under various confining pressures. The range of particle size variation increases with increasing confining pressure, except for particles between 5 and 20 mm. The particle content is significantly affected by high confining pressure, particularly for particles with a size of 20–60 mm, which shows a change range of approximately 40% and a more pronounced impact on larger particle sizes.

To illustrate the impact of dry density on particle breakage, a histogram is created. The figure shows the composition of each particle group at a confining pressure of 400 kPa and varying dry densities. Figure 11 shows how particle breakage increases as the dry density increases during the test at a confining pressure of 400 kPa. This is because the sample becomes denser at higher dry densities, making relative movement between particles more difficult and increasing the likelihood of breakage [30]. The degree of change in the particle breakage is consistent regardless of the confining pressure, with a more pronounced change ranging as the dry density increases.

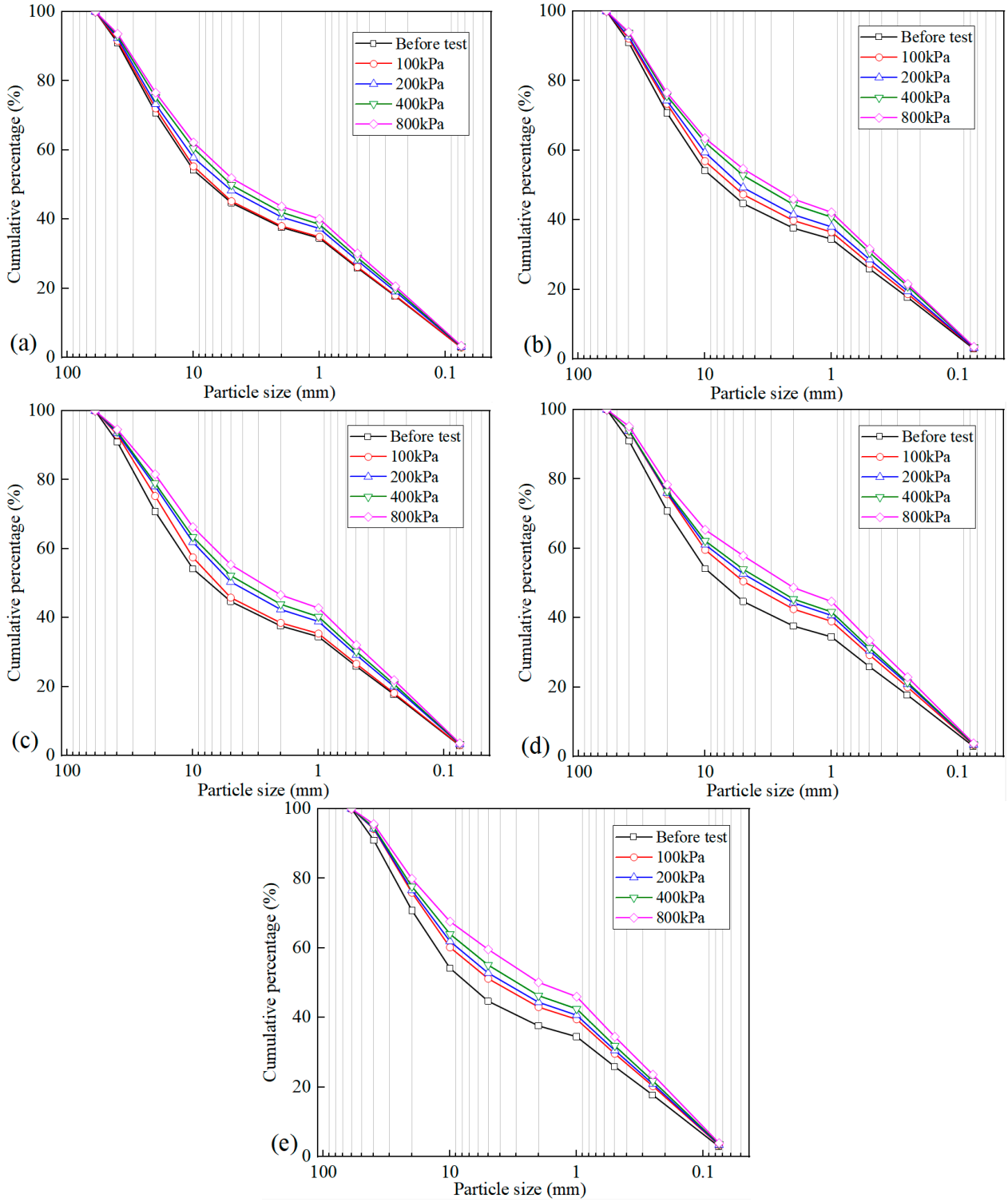

Figure 9. Grading curve of the soil-rock mixture before and after shearing: (**a**) dry density of 1.76 g/cm^3, (**b**) dry density of 1.82 g/cm^3, (**c**) dry density of 2.00 g/cm^3, (**d**) dry density of 2.15 g/cm^3, and (**e**) dry density of 2.30 g/cm^3.

Table 2. Screening results of S-RMS after shearing.

ρ_d (g/cm^3)	σ_3 (kPa)	Different Particle Size of Each Particle Group Content (%)								
		60~40 mm	40~20 mm	20~10 mm	10~5 mm	5~2 mm	2~1 mm	1~0.5 mm	0.5~0.25 mm	<0.25 mm
Before test		9.00	20.20	16.60	9.50	7.10	3.10	8.60	8.20	17.70
1.76	100	8.40	19.50	16.70	10.20	7.20	3.10	8.70	8.30	17.90
	200	7.60	19.10	15.50	9.50	7.70	3.30	9.30	8.90	19.10
	400	7.00	17.70	14.80	10.50	7.90	3.50	9.60	9.20	19.80
	800	6.40	17.00	14.40	10.30	8.20	3.60	10.00	9.50	20.60
1.82	100	7.90	18.70	16.40	9.60	7.50	3.30	9.10	8.70	18.80
	200	7.30	18.40	14.90	10.10	7.80	3.40	9.50	9.00	19.60
	400	6.20	18.10	13.40	9.50	8.40	3.70	10.20	9.70	20.80
	800	6.00	17.40	13.10	8.90	8.70	3.80	10.50	10.00	21.60
2.00	100	6.90	17.70	17.80	11.70	7.30	3.20	8.80	8.40	18.20
	200	6.50	15.50	16.20	11.40	8.00	3.50	9.70	9.30	19.90
	400	6.00	14.90	15.70	11.20	8.30	3.60	10.00	9.60	20.70
	800	5.40	13.00	15.30	10.90	8.80	3.80	10.70	10.20	21.90
2.15	100	6.20	18.20	16.00	9.10	8.00	3.50	9.70	9.30	20.00
	200	6.10	17.90	14.90	8.40	8.40	3.70	10.10	9.80	20.70
	400	6.00	17.50	14.30	8.10	8.60	3.70	10.40	9.90	21.50
	800	4.80	16.80	13.10	7.50	9.20	4.00	11.10	10.60	22.90
2.30	100	5.80	18.30	15.70	9.10	8.10	3.50	9.80	9.40	20.30
	200	5.70	17.70	14.70	9.10	8.40	3.70	10.20	9.70	20.80
	400	5.30	16.90	13.70	8.90	8.70	3.80	10.60	10.10	22.00
	800	4.40	15.70	12.30	8.00	9.50	4.10	11.50	10.90	23.60

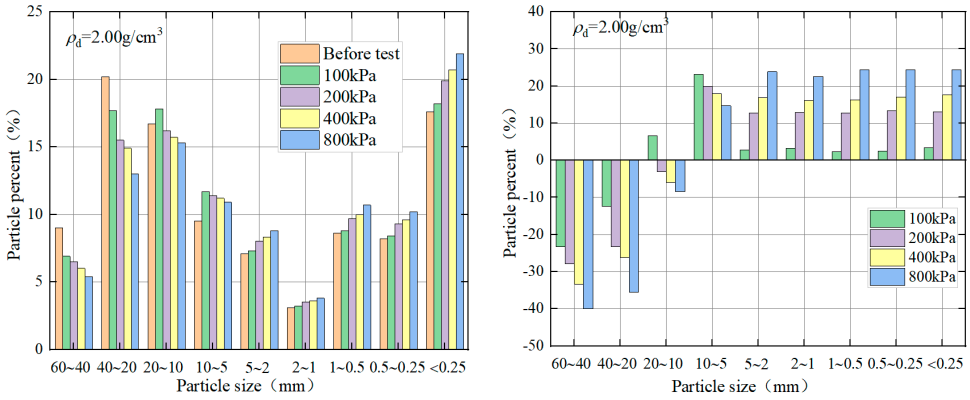

Figure 10. Histogram of the content of each granule with a density of 2.00 g/cm^3. (**a**) Histogram of the content of each grain group. (**b**) Histogram of the content change of each grain group.

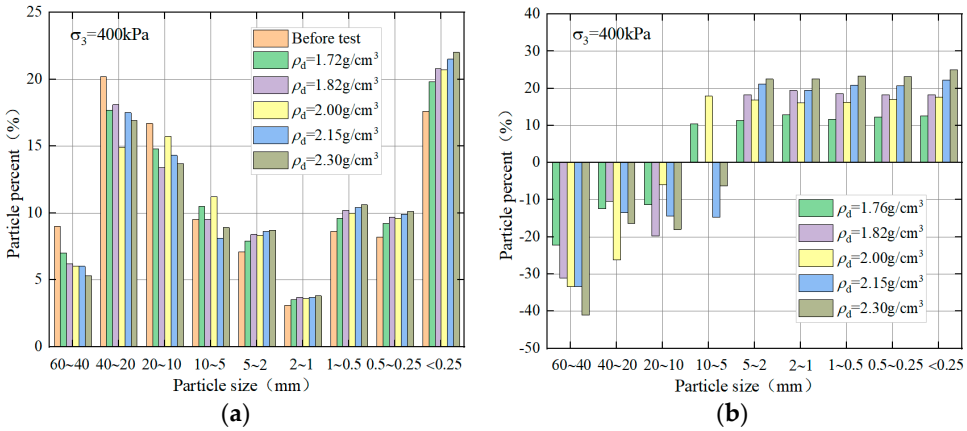

Figure 11. Histogram of the content of each granule at a confining pressure of 400 kPa. (**a**) Histogram of the content of each grain group. (**b**) Histogram of the content change of each grain group.

3.4. Analyzing the Particle Breakage Characteristics of Soi-Rock Mixtures Using an Improved Particle Breakage Index, B_C

Figure 9 displays the grading curves before and after shearing for five groups with varying dry densities under different confining pressures. The curves for each confining pressure at various dry densities were integrated, and the breakage index B_C for each confining pressure was determined using Equation (2). The breakage index B_C can be found in Table 3.

Table 3. Calculation results of the particle breakage index.

ρ_d (g/cm^3)	σ_3 (kPa)	D	B_C (%)
Before test	/	2.7080	/
1.76	100	2.7086	0.94
	200	2.7215	2.40
	400	2.7264	3.93
	800	2.7335	5.05
1.82	100	2.7174	2.15
	200	2.7248	3.40
	400	2.7380	5.31
	800	2.7448	6.16
2.00	100	2.7075	3.09
	200	2.7260	5.56
	400	2.7322	6.57
	800	2.7431	8.62
2.15	100	2.7286	4.54
	200	2.7376	5.24
	400	2.7427	5.82
	800	2.7554	8.05
2.30	100	2.7309	4.98
	200	2.7370	5.76
	400	2.7452	6.97
	800	2.7601	9.31

Table 2 provides the grading of each particle size after shearing, and the fractal dimension D can be determined using Equation (3). Figure 12 shows a diagram of the fractal dimension results for the five groups at the various dry densities. The fitting plots of the fractal dimensions D of the five groups with different dry densities showed consistent trends, and the results of the fractal dimensions D are listed in Table 3.

Table 3 shows the computed values of sample fractal dimension D and particle breakage index B_C at various dry densities. Table 3 clearly shows that both the fractal dimension D and the breakage index B_C increase as the confining pressure increases.

The improved breakage index B_C and fractal dimension D were utilized to describe the particle breakage degree based on the area of the gradation curve and fractal characteristics, respectively, according to the particle size distribution characteristics. The fractal dimension D and the breakage index B_C were fitted. A strong linear regression link between the fractal dimension D and the breakage index B_C is demonstrated in Figure 13, with a correlation coefficient R^2 of 0.96. The improved breakage index B_C and fractal dimension D can indicate the particle distribution features inside the soil-rock mixture at varying degrees of breakage. Both methods are effective in describing and measuring the degree of particle breakage, aligning with the findings of previous studies [5,23].

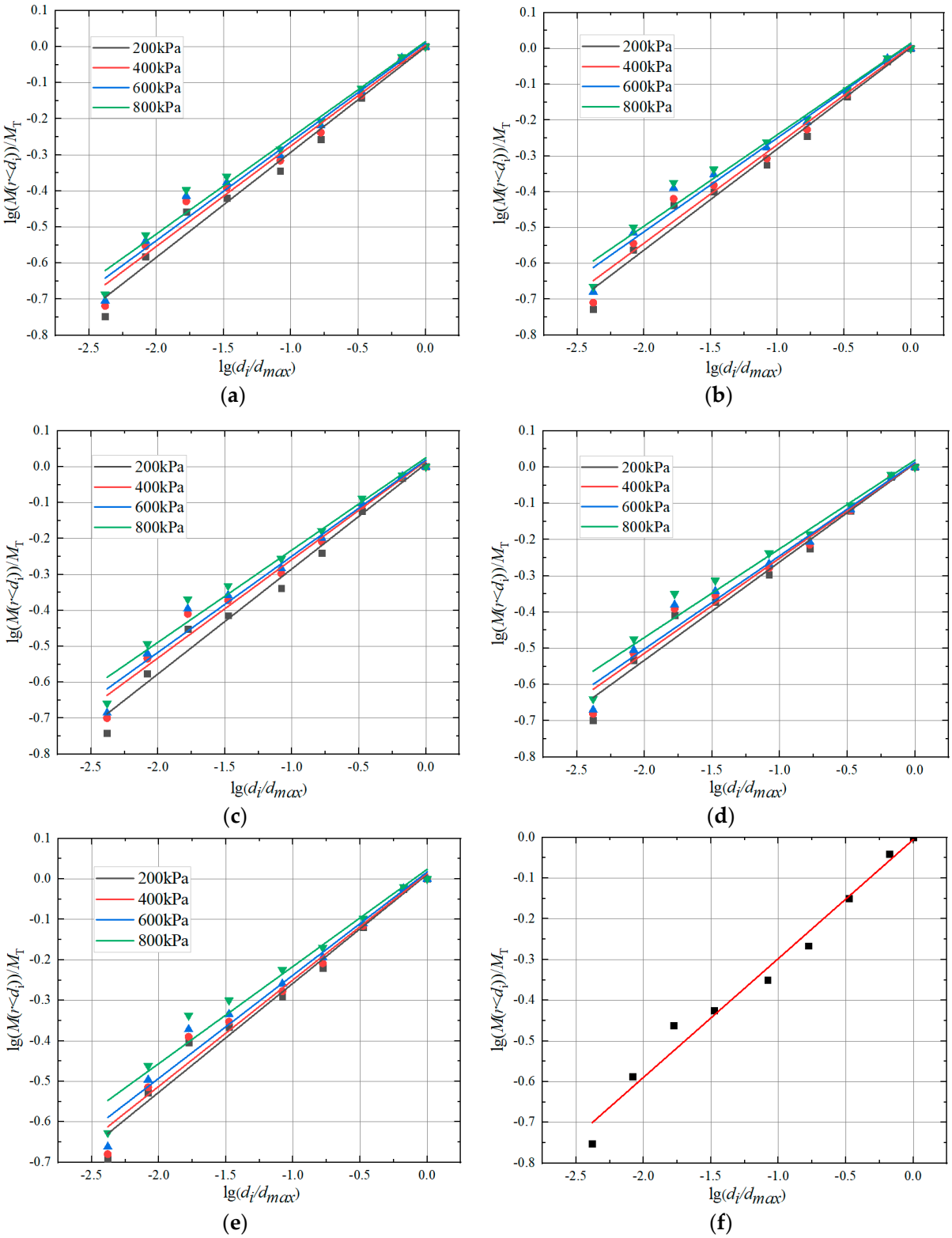

Figure 12. Fractal dimension D fitting diagram: (**a**) dry density of 1.76 g/cm^3, (**b**) dry density of 1.82 g/cm^3, (**c**) dry density of 2.00 g/cm^3, (**d**) dry density of 2.15 g/cm^3, (**e**) dry density of 2.30 g/cm^3, and (**f**) before test.

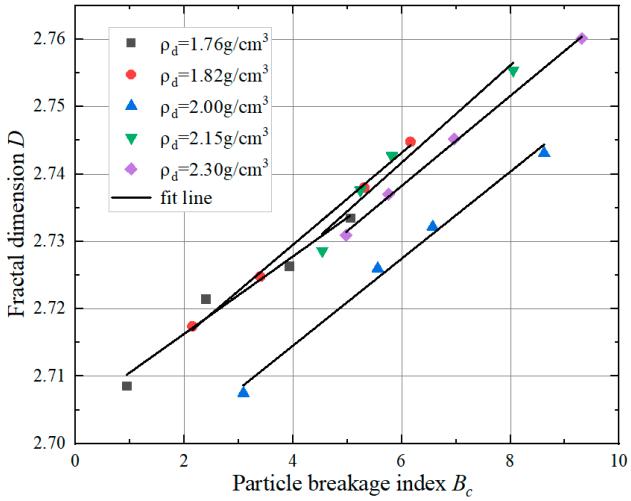

Figure 13. The relationship between fractal dimension D and fragmentation index B_C.

4. Analyzing the Impact of the Particle Breakage Index B_C on the Deformation Strength Characteristics

4.1. Analyzing the Impact of the Breakage Index B_C on the Deformation Characteristics

The dilatancy of a soil-rock mixture is described by the dilatancy rate, which is defined as, $\zeta = d\varepsilon_v^p / d\varepsilon_a^p$, representing the ratio of the plastic volumetric strain increment to the plastic partial strain increment. The sample's volume exhibits a relative dilatation deformation trend (dilatancy rate $d\varepsilon_v^p / d\varepsilon_s^p < 0$) during the shear process, known as dilatancy, as per the definition provided above. Guo et al. [31] analyzed the triaxial CD test results of coarse-grained soil to compare the plastic strain increase ratio with the total strain increase ratio. They discovered that the dilatation ratio was minimally affected by elastic strain. Hence, the dilatation ratio of $d\varepsilon_v^p / d\varepsilon_s^p$ can be represented as $d\varepsilon_v / d\varepsilon_s$, and the general form of the dilatation equation was derived. $d\varepsilon_v / d\varepsilon_s$ is utilized to characterize the dilatancy of soil-rock mixtures in this paper.

The dilatancy of soil material is influenced by its initial physical and mechanical state, which refers to the change in soil volume due to shear [32]. The main focus of this paper is to study the impact of various dry densities on particle breakage characteristics. The dry density and initial void ratio exhibit a negative correlation. By transforming dry density into the initial void ratio, relevant data on dry density can be indirectly acquired. The failure dilatancy rate ζ_f and particle breakage index B_C were plotted on a two-dimensional plane under various initial void ratios. As shown in Figure 14, under the same initial void ratio, the failure dilatancy rate gradually increases with increasing breakage index B_C. This study indicates that the size of the soil-rock mixture decreases as the number of particle breakages increases. During shearing, the staggered tumbling amplitude of the particles decreases, resulting in a decrease in shear volume dilatation and a transition from shear dilatation to shear shrinkage.

After fitting the scattered points, it was found that there is a strong power function correlation between the failure dilatancy rate and the particle breakage index [33], expressed as:

$$\zeta_f = mB_c^n \tag{13}$$

where m and n are parameters that are adjusted to fit the data.

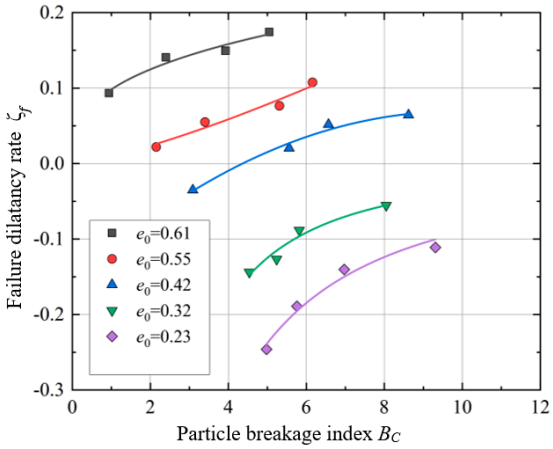

Figure 14. Relationship curve between the breakage index and failure dilatancy rate.

4.2. Analyzing the Impact of the Breakage Index B_C on the Strength Characteristics

By studying the phenomena and laws of particle breakage, it is evident that particle breakage, density, and confining pressure significantly influence the strength characteristics of soil-rock mixtures. The linear Mohr-Coulomb strength criterion is commonly used for stability analysis. When dealing with soil-rock mixtures, it is important to consider cohesion when determining the internal friction angle.

The Mohr-Coulomb strength criterion is employed to determine the cohesion in a linear manner. Soil materials typically fail through shear failure, and Coulomb suggested the following equation for shear strength:

$$\tau_f = c + \sigma \tan \varphi \tag{14}$$

where τ_f represents the shear strength, σ represents the normal stress, c represents the cohesion, and φ represents the internal friction angle. According to the data in Table 4, the Mohr circle and strength envelope under different dry densities are drawn.

Table 4. Peak shear stress and shear strength index under different dry densities.

Number	ρ_d g/cm^3	$(\sigma_1 - \sigma_3)_f$ kPa			
		100	200	400	800
1	1.76	473.2	770.1	1350.8	2311.8
2	1.82	548.8	906.5	1520.8	2610.8
3	2.00	805.2	1085.6	1782.2	3083.1
4	2.15	812.7	1150.3	1832.9	3196.0
5	2.30	978.7	1383.9	2095.6	3587.4

The internal friction angle estimates for large particles or rockfill made of weak minerals or weathered rocks clearly show a nonlinear strength envelope. When analyzing the stability of a waste slag rockfill dam, it is important to consider the nonlinear characteristics of the strength envelope of the soil-rock mixture under high confining pressure [34]. Assuming that the cohesion of the same dry density is constant, the internal friction angle is calculated using the nonlinear equation of the strength envelope. The nonlinear equation of the strength envelope [35,36] is as follows:

$$\tau_f = c + \sigma \tan(\varphi_0 - \Delta\varphi lg\tfrac{\sigma_3}{p_a}) \tag{15}$$

where φ represents the angle of internal friction when the continuous cohesion is extended in reverse to the point where the axis intersects the Mohr circle. represents the angle of internal friction under a pressure of one atmosphere. $\Delta\varphi$ is a nonlinear parameter that signifies the reduction in φ over a logarithmic period as σ_3 increases. p_a represents the

atmospheric pressure, with a value of 101.3 kPa, which has the same unit as σ_3. The values for φ, φ_0, $\Delta\varphi$ and c can be found in Table 5. At the same time, draw the Mohr circle and strength envelope of the sample with dry density of 1.82 g/cm^3, as shown in Figure 15.

Table 5. Shear strength parameters of samples with different dry densities.

ρ_d (g/cm^3)	σ_3 (kPa)	φ	φ_0	$\Delta\varphi$	c/kPa
1.76	100	36.63	36.55	1.72	57
	200	36.33			
	400	36.00			
	800	35.01			
1.82	100	38.55	38.44	2.23	73
	200	38.10			
	400	37.66			
	800	36.46			
2.00	100	40.86	40.60	2.46	109
	200	39.42			
	400	39.30			
	800	38.43			
2.15	100	41.45	41.34	2.71	112
	200	40.51			
	400	39.72			
	800	39.20			
2.30	100	43.85	43.76	3.14	127
	200	43.09			
	400	41.66			
	800	41.11			

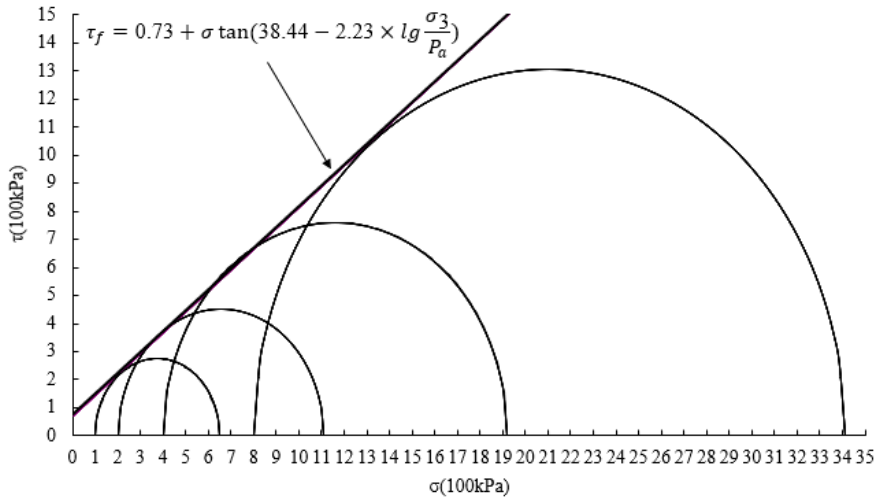

Figure 15. Mohr circle and strength envelope diagram of sample with dry density of 1.82 g/cm^3.

Figure 16 displays the relationship curves between the confining pressure σ_3 and internal friction angle φ at different densities, based on the data in Table 5. At a constant confining pressure σ_3, increasing the dry density results in a greater internal friction angle φ, more pronounced interparticle occlusion, and greater shear strength. The internal friction angle of the soil-rock mixture mostly originates from the sliding friction of particle surfaces and the occlusion friction between particles. As the confining pressure σ_3 increases in this process, the binding force also increases, making it harder for particles to move across, leading to more severe particle breakage and increased particle breakage. As the bite force between particles diminishes, the internal friction angle φ and shear strength also decrease. At the same time, increasing the dry density results in a higher nonlinear parameter $\Delta\varphi$ and leads to a greater nonlinear shear strength of the sample.

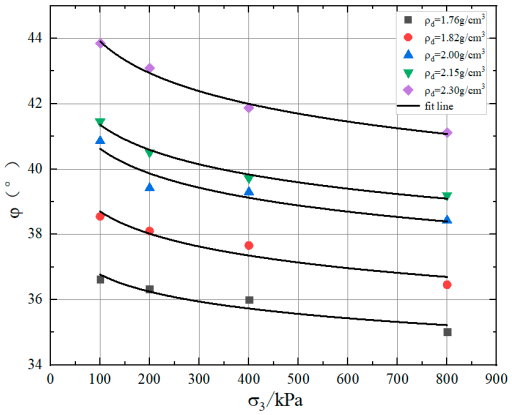

Figure 16. Relationships between the confining pressure σ_3 and internal friction angle φ.

The analysis presented in Figure 16 demonstrates that as the confining pressure increases, particle breakage intensifies, resulting in a slower reduction in the internal friction angle φ. Overall, the internal friction angle exhibits a nonlinear trend. This is because with a further increase in the confining pressure, particle breakage or deformation occurs, leading to changes in the surface shape and structure of some particles. Consequently, the magnitude and distribution of the friction force also change. The contact region between soil particles tends to become saturated, and further increasing the confining pressure has little effect on the soil. Therefore, particle breakage is a significant contributing factor to the nonlinear trend of the internal friction angle.

Figure 17 displays the correlation between the breakage index B_C, fractal dimension D, and internal friction angle φ at various dry densities. Figure 17a illustrates a clear correlation between the particle breakage and internal friction angle φ. At the same dry density, with increasing breakage index B_C, the internal friction angle φ gradually decreases, and the internal friction angle φ exhibits a nonlinear trend, which is consistent with the conclusion of the above relationship curve between the confining pressure σ_3 and the internal friction angle φ. For fractal dimension D, the larger the fractal dimension D, the higher the degree of breakage [15]. As can be seen from Figure 17b, with the increase in fractal dimension d, the internal friction angle also shows a decreasing trend. Comparing the two relationship curves shows that the decreasing trend of the internal friction angle φ is similar under different dry densities in both panels of Figure 17a,b, indicating the rationality of using the improved breakage index B_C to analyze the strength characteristics.

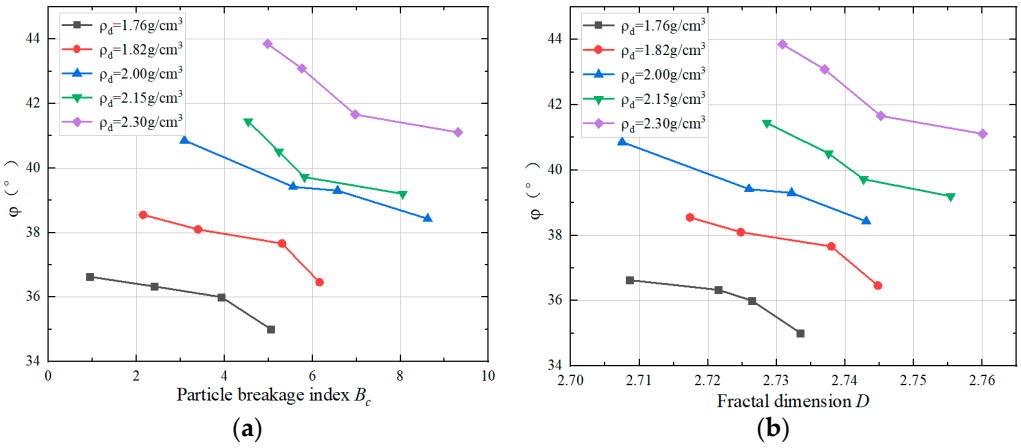

Figure 17. Relationship between the internal friction angle and the particle breakage index. (**a**) Relationship curve between the breakage index and internal friction angle. (**b**) Relationship curve between the fractal dimension and the internal friction angle.

5. Conclusions

Based on the previous breakage index, the improved breakage index B_C was established in this paper. Through the quantitative relationship with the fractal dimension, the rationality of the improved breakage index B_C was explained. Based on large-scale triaxial shear test results of soil-rock mixtures under different dry densities, the following conclusions were drawn:

(1) Combined with the phase transformation stress ratio M_{pt}, when the dry density increases, the phase transformation stress ratio M_{pt} also increases, leading to an increase in the volume variable. As the confining pressure increases, M_{pt} decreases progressively, suggesting a decrease in the volume variable, and the specimen exhibits dilatancy hysteresis.

(2) The particle breakage increases with increasing confining pressure before and after particle-grading shear. The largest changes in particle breakage occur in the particle group ranging from 20 to 60 mm. A higher dry density leads to more noticeable particle breakage. The breakage index B_C and fractal dimension D are fitted, resulting in well-fitting parameters that effectively describe and quantify the overall degree of particle breakage.

(3) In the study of deformation characteristics, the failure dilatancy rate ζ_f shows a strong power function correlation with the particle breakage index B_C. The absolute value of the failure dilatancy rate ζ_f decreases with increasing crushing index B_C, transitioning gradually from dilatancy to shear shrinkage.

(4) When investigating the strength characteristics, increasing the confining pressure also increases the breakage index B_C. This leads to a decrease in the internal friction angle and a decrease in the shear strength, exhibiting a nonlinear trend. Particle breakage is the direct cause that affects the nonlinearity of the internal friction angle.

Author Contributions: Supervision, Funding acquisition, Writing—review and editing: P.X.; Investigation, Methodology, Writing—original draft: Z.C.; Conceptualization, data curation: L.F.; Funding acquisition, Investigation, Revision: Z.X.; Supervision, Revision, Conceptualization: Q.L.; Supervision, Revision, Conceptualization: Z.L. All authors have read and agreed to the published version of the manuscript.

Funding: National Natural Science Foundation of China (52179143); Natural Science Basic Research Program of Shaanxi Province (2023-JC-YB-383); Key Industry Innovation Chain of Shaanxi (2022ZDLNY02-04).

Institutional Review Board Statement: Not applicable.

Informed Consent Statement: Not applicable.

Data Availability Statement: The data presented in this study are openly available in China National Knowledge Infrastructure at https://doi.org/10.27398/d.cnki.gxalu.2023.001199 (accessed on 2 July 2024).

Conflicts of Interest: The authors declare no conflicts of interest.

References

1. Marsal, R.J. Mechanical properties of rockfill. In *Embankment Dam Engineering Casagrande Volume*; Wiley: New York, NY, USA, 1973.
2. Hardin, B.O. Breakage of soil particles. *J. Geotech. Eng.* **1985**, *111*, 1177–1192. [CrossRef]
3. Einav, I. Breakage mechanics—Part i: Theory. *J. Mech. Phys. Solids* **2007**, *55*, 1274–1297. [CrossRef]
4. Wu, E.L.; Zhu, J.G.; Huang, W.; Liu, Z. Evolution law of particle breakage of coarse-grained soil during triaxial shearing. *Chin. J. Geotech. Eng.* **2020**, *42*, 2330–2335.
5. Guo, W.L.; Zhu, J.G.; Wang, Q.L.; Yu, T. Mathematical model based on the gradation equation for predicting gradation evolution of coarse-grained soils. *J. Cent. South Univ. (Sci. Technol.)* **2018**, *49*, 2076–2082.
6. Tao, Q.D.; He, Z.Y.; Jia, Y. Strength Characteristics and Influencing Factors of Soil-rock Mixture Based on Large Triaxial Test. *Sci. Technol. Eng.* **2019**, *19*, 310–318.
7. Tu, Y.L.; Liu, X.R.; Ren, Q.Y.; Chai, H.J.; Wang, J.B.; Yu, J.Y. Effects of rock contents and particle breakage on strength characteristics of soil-rock aggregate. *Rock Soil Mech.* **2020**, *41*, 3919–3928.
8. Lei, X.D.; Yang, Z.P.; Zhang, X.J.; Tu, Y.L.; Liu, S.L.; Hu, Y.X. Shear properties and rock block breakage characteristics of soil-rock mixtures. *Rock Soil Mech.* **2018**, *39*, 899–908+916.

9. Yang, S.; Li, X.Q. Simulation Analysis of Large Direct Shear Test of Soil and Rock Mixture Based on PFC3D. *Adv. Eng. Sci.* **2020**, *52*, 78–85.
10. Hu, W.; Dano, C.; Hicher, P.-Y.; Le Touzo, J.-Y.; Derkx, F.; Merliot, E. Effect of sample size on the behavior of granular materials. *Geotech. Test. J.* **2011**, *34*, 103095. [CrossRef]
11. Jiang, M.J.; Ji, E.Y.; Wang, T.C.; Li, S.; Zhu, J.; Mei, G. Experimental study on laws of scale effects of shear strength of coarse-grained soils. *Chin. J. Geotech. Eng.* **2023**, *45*, 855–861.
12. Cai, Z.Y.; Li, X.M.; Guan, Y.F.; Huang, Y.H. Particle breakage rules of rockfill materials. *Chin. J. Geotech. Eng.* **2016**, *38*, 923–929.
13. Guo, W.L.; Zhu, J.G.; Qian, B.; Zhang, D. Particle breakage evolution model of coarse-grained soil and its experimental verification. *Rock Soil Mech.* **2019**, *40*, 1023–1029.
14. Wu, X.L.; Shi, B.X.; Liu, S.C.; Xu, W.W.; Chang, W.K. Large-scale Triaxial Test of Rockfill Material Considering Particle Breakage. *Sci. Technol. Eng.* **2022**, *22*, 749–756.
15. Liang, P.; Yang, Y.; Huang, H.; Liu, J.; Guo, N. Experimental Study on Fractal Characteristics of Particle Size Distribution by Repeated Compaction of Road Recycling Crushed Stone. *Appl. Sci.* **2022**, *12*, 10303. [CrossRef]
16. Shi, Z.M.; Zhao, X.W.; Peng, M. Review of Studies on Large Scale Triaxial Tests of Coarse-Grained Soils. *J. Eng. Geol.* **2014**, *22*, 792–796.
17. Liu, M.C.; Meng, F.; Wang, Y.Y. Evolution of particle crushing of coarse-grained materials in large-scale triaxial tests. *Chin. J. Geotech. Eng.* **2020**, *42*, 561–567.
18. Yu, F. Particle breakage in granular soils: A review. *Part. Sci. Technol.* **2021**, *39*, 91–100. [CrossRef]
19. Muir Wood, D.; Maeda, K. Changing grading of soil: Effect on critical state. *Acta Geotech.* **2008**, *3*, 3–14. [CrossRef]
20. Mandelbrot, B.B.; Wheeler, J.A. The fractal geometry of nature. *Am. J. Phys.* **1983**, *51*, 286–287. [CrossRef]
21. Du, J.; Hou, K.P.; Liang, W.; Peng, G.C. Experimental study of compaction characteristics and fractal feature in breakage of coarse-grained soils. *Rock Soil Mech.* **2013**, *34*, 155–161.
22. Tyler, S.W.; Wheatcraft, S.W. Fractal scaling of soil particle-size distributions: Analysis and limitations. *Soil Sci. Soc. Am. J.* **1992**, *56*, 362–369. [CrossRef]
23. Shi, X.S.; Cheng, Z.L. fractal behavior in crushing of rockfill material. *Chin. J. Rock Mech. Eng.* **2010**, *29*, 3852–3857.
24. Ding, L.N.; Li, G.Y. SBG model for particle breakage of rockfills based on fractal gradation equation. *Chin. J. Geotech. Eng.* **2022**, *44*, 264–270.
25. *GB/T 50123-2019*; Standard for Geotechnical Testing Method. Chinese Standard: Beijing, China, 2019. (In Chinese)
26. Manzari, M.T.; Dafalias, Y.F. A critical state two-surface plasticity model for sand. *Géotechnique* **1997**, *47*, 255–272. [CrossRef]
27. Liu, H.L.; Qin, H.Y.; Gao, Y.F.; Zhou, Y.D. Experimental study on particle breakage of rockfill and coarse aggregates. *Rock Soil Mech.* **2005**, *26*, 562–566.
28. Guo, Y.; Zhang, J.; Li, M.; Timms, W.; Shen, L.; Li, P. Effects of Loading Stress and Velocity on Compression and Particle Breakage Behaviour of Waste Rocks in Backfill Coal Mining. *Appl. Sci.* **2022**, *12*, 11175. [CrossRef]
29. Liu, Y.; Yu, P.Q.; Zhang, D.; Wang, X.X. Micromechanics-based stress-dilatancy relationship for granular materials. *Chin. J. Geotech. Eng.* **2021**, *43*, 1816–1824.
30. Cai, Z.Y.; Hou, H.Y.; Zhang, J.X.; Zhang, F.; Guan, Y.; Cao, Y. Experimental study on the influence of density and stress level on particle breakage of coral sand. *Shuili Xuebao* **2019**, *50*, 184–192.
31. Guo, W.L.; Zhu, J.G.; Peng, W.M. Dilatancy equation and generalized plastic constitutive model for coarse-grained soils. *Chin. J. Geotech. Eng.* **2018**, *40*, 1103–1110.
32. Cai, Z.Y.; Zhong, Q.M.; He, N.; Xia, Y.F.; Zhu, J.G. Research Framework of the State-dependent Dilatancy Theory and Breach Evolution Law of Landslide Dam. *Adv. Eng. Sci.* **2021**, *53*, 21–32.
33. Shi, B.X.; Liu, S.C.; Wu, X.L.; Chang, W.K. Dilatancy behaviors of rockfill materials considering particle breakage. *Chin. J. Geotech. Eng.* **2021**, *43*, 1360–1366.
34. Zhang, Z.P.; Fu, X.D.; Sheng, Q.; Yin, D.; Song, D.; Du, Y. A non-linear ultimate strength criterion for soil-rock mixture based on rock block proportion. *Chin. J. Rock Mech. Eng.* **2021**, *40*, 1672–1686.
35. Duncan, J.M.; Byrne, P.; Wong, K.S.; Mabry, P. Strength, stress-strain and bulk modulus parameters for finite element analyses of stresses and movements in soil masses. *J. Consult. Clin. Psychol.* **1980**, *49*, 554–567.
36. Liu, X.R.; Tu, Y.L.; Wang, P.; Zhong, Z.L.; Tang, W.B.; Du, L.B. Particle breakage of soil-rock aggregate based on large-scale direct shear tests. *Chin. J. Geotech. Eng.* **2017**, *39*, 1425–1434.

Disclaimer/Publisher's Note: The statements, opinions and data contained in all publications are solely those of the individual author(s) and contributor(s) and not of MDPI and/or the editor(s). MDPI and/or the editor(s) disclaim responsibility for any injury to people or property resulting from any ideas, methods, instructions or products referred to in the content.